JOURNAL OF MATERIALS SCIENCE **34** (1999) 5557–5567

Microstructural nature of strengthening and toughening in Al_2O_3-$SiC_{(p)}$ nanocomposites

C. C. ANYA
*37 Beech Crescent, Kidlington, Oxford OX5 1DP. United Kingdom**
E-mail: c.anya@urjgin.net

It is demonstrated that neither of the theories based on flaw size, surface flaw healing or residual stress adequately and consistently explain the strengthening and toughening phenomena in Alumina-SiC nanocomposites. SiC presence reduces the amount of amorphous (glassy) silica rich phase (SRP) in the nanocomposite relative to that found in monolithic Alumina and to a level that the effect of SRP is negligible. The reduction of SRP and the multipliable effect of microstructural features such as dislocations, crack/particle interactions and cleavage steps, observed in these materials at an extraordinarily small scale (due to the nano-size of the SiC particles), are suggested to be more consistent in explaining these phenomena. Owing to the nano-scale at which these features operate, which is far below the practical resolution limit of the Scanning Acoustic Microscope (SAM), it is also argued that the latter may not be a good method for studying these materials.

1. Introduction

It was reported [1] that the same level of strength is achieved after annealing ground, and ground-polished (hereafter referred to as "polished") samples of Al_2O_3-5 vol % $SiC_{(p)}$ nanocomposite, Table I. The work concluded that the healing of available surface defects (flaws) is responsible for the increase in strength found in the nanocomposite. Small cracks (flaws) are more healable than the relatively large ones. If healing of surface flaws were responsible, considering that relative to the ground samples more healable flaws are found in the polished ones, Fig. 1 [2, 3], the latter should have shown higher strength after annealing. The fact that they do not suggest that under these conditions other mechanisms, apart from sizes and the healing of surface flaws, control strengthening in these materials.

On the basis of Hertzian indentation results it was also suggested [1] that the intrinsic toughness, $K_{1C(Hertz)}$, of monolithic Alumina and 5 vol % SiC-Alumina nanocomposite of a similar grain size to be very similar. The work further suggested that the higher $K_{1C(Hertz)}$ value observed for the composite in an earlier work [2] is rather due to residual stresses (accruing from the machining process) in its surface. Using interferograms Chou *et al*. [4] demonstrated that both the nanocomposite and Alumina showed similar quantitative response to machining. Thus there is no difference in the magnitude of residual stress in both materials when machined. Therefore the observed [2] higher $K_{1C(Hertz)}$ of the nanocomposite cannot be attributed to a non-existent residual stress difference. The similarity between the $K_{1C(Hertz)}$ of the annealed Alumina and the nanocomposite [1] may be due to changes in the elastic properties (on which $K_{1C(Hertz)}$ depends [1, 2]) resulting from the formation of a reactive layer, claimed [1] to be amorphous mullite on the surfaces of the nanocomposite samples.

However, the Hertzian indentation test, ideally, is stopped at the instance a crack is initiated (indicated by an acoustic emission) from an existing flaw. Hence the toughness values derived from this method do not take into account the possible effect of interaction of microstructural features with a crack propagating to the point the entire material fails. Using methods based on bulk sample tests, several authors [5–11] have demonstrated that 5% SiC-Alumina nanocomposite's bulk toughness, K_{1C} values are higher than that of monolithic Alumina. The toughening aspect of this work concentrates on K_{1C}.

Using Vickers indentation method the higher values of K_{1C} in 5 vol % SiC-Alumina nanocomposite (relative to Alumina) was suggested [12] to be due to compressive residual stresses from machining processes. Using the same indentation method the graph of K_{1C} vs. crack lengths for Alumina, 5 and 10 vol % SiC nanocomposites, Fig. 2 (an approach used by Ikuma and Virkar [13]), the residual stress hypothesis [12] is not supported. In this figure, the gradient (b) represents the magnitude of surface residual stress, and it can be seen that though the residual stress is least in the 10 vol % SiC nanocomposite, it shows the highest K_{1C} value.

Thus explanations of the strengthening and toughening of nanocomposites, relative to Alumina, based on residual stresses, healable flaws and properties of their

* This work was carried out at University of Oxford, Department of Materials, Oxford OX1 3PH United Kingdom.

TABLE I Strengths achieved for 5 vol % SiC nanocomposite with different surface conditions and treatment (ref. [1])

Surface condition	Treatment	Strength (MPa)
Ground	Unannealed	395 ± 120
Ground and polished	Unannealed	540 ± 60
Ground	Annealed, 2 h	615 ± 65
Ground	Annealed, 10 h	680 ± 50
Ground and polished	Annealed, 10 h	615 ± 65

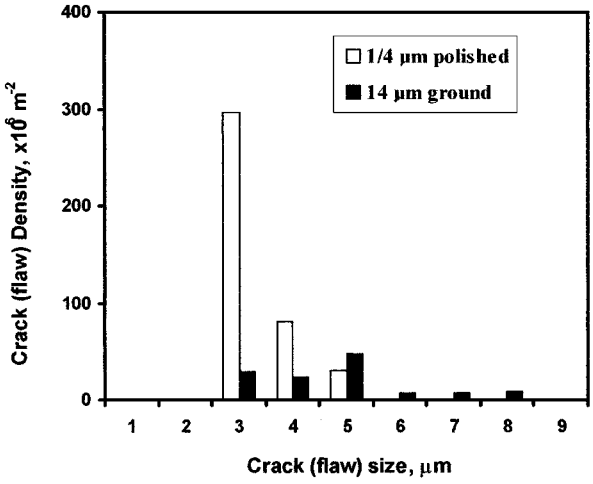

Figure 1 Density of flaws vs. flaw sizes for ground and polished samples of 5% SiC composite. Note that flaws of smaller sizes and higher density predominate in polished samples.

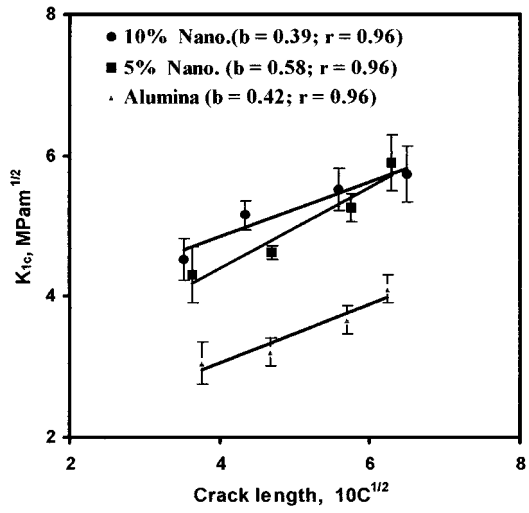

Figure 2 Vickers indentation fracture toughness, K_{1C} vs. crack length ($C^{1/2}$). Note that the gradient, b, (indicative of the magnitude of the residual stress in the samples) is least for 10% SiC composite that shows the highest K_{1C} value.

degraded surfaces are ambiguous and inconsistent with experimental observations.

Modern technologies demand a first-time-right approach, because it saves time and resources. This can be achieved by mathematical modelling. In any case such a model has to be practically relevant, which therefore, in the first instance, requires an unambiguous understanding of the fundamental basis of the phenomena involved. No mathematical modelling is undertaken in this work. However, to minimise or eliminate the ambiguities so far met in explaining the phenomena in this system, it was felt that a thorough attention is given to the role of microstructural features in the strengthening and toughening of $Al_2O_3/SiC_{(p)}$ nanocomposites (relative to Alumina). This is the focus of the present work, and it is mostly at nano-scale to correspond with the scale of the particles. The reduction in strenth at additions more than 5 vol % SiC in the composites is also explained on this basis. The initial surface chemistry of SiC (and the content of silica rich phases—SRP—in Alumina) is also briefly considered since it has been shown [5] that this could contribute to the strength of interfaces.

2. Materials and experimental methods

The monolithic Alumina, and 5, 10, and 15 vol % SiC 'nanocomposites' were pressureless sintered to $\geq$99.6 % theoretical density at 1775 °C. The average particle sizes of the Alumina and SiC powders were respectively 400 and 200 nm. The size distribution of SiC particles ranges from about 100 to 900 nm, with a d_{50} value of about 200 nm. Prior to sintering, the powders were blended by attrition milling in water, freeze-dried and isostatically cold-pressed. In Table II are the characteristics of the Alumina and α-SiC (Lonza 45), as determined by the suppliers. Full details of the fabrication process have been reported elsewhere [14]; in brief, the equation,

$$SiO_2 + C \rightarrow SiO + CO \qquad (1)$$

is more thermodynamically favourable than the reaction of SiC with SiO_2 [14] during sintering. This equation suggests that 1 wt % SiO_2 requires about 0.2 wt % C to be completely reduced to gaseous constituents that escape from the sintered samples. If it is assumed that the entire Si metal contained in the SiC powder (Table II) is in the form of amorphous SRP film on SiC particles, there will be about 0.47 wt % of SiO_2 associated with the Silicon present. Following from Equation 1 this amount will require about 0.1 wt % C to be completely reduced. This is well taken care of by the 0.58 wt % free carbon contained in the SiC powder. Hence it could be said that the amorphous film of SRP on the particles is completely reduced. However, the Alumina powder also contains amorphous silica rich phases. From the background hump of the XRD (between a 2θ value of about 7° and 15°) that is shown in Fig. 3, it can be seen the free carbon in the SiC powder also reduces this significantly. This reduction, coupled with the very low content of SiO_2 in the Alumina justifies considering that the amount of SRP in the composites is insignificant to have any major impact on the flexural strength of the composites.

Four-point bend test samples of $25 \times 2.5 \times 2$ mm were made by grinding and polishing sections cut out from discs of 40 mm diameter by 6 mm thickness. The tensile faces were polished to 1/4 μm finish, while the other two sides were polished to 1 μm finish. A very important aspect of the preparation of these samples is the chamfering of the tensile edges. This was carried

TABLE II Characteristics of raw materials

Materials	Characteristics (suppliers) (wt %)											
	Al_2O_3	SiO_2	Fe_2O_3	Na_2O	MgO	CaO	Mean particle size (μm)	Density ($g\,cm^{-3}$)	Free *C*	Fe_2O_4	Si Metal	O_2
α-Al_2O_3	99.9	0.04	0.01	0.03	0.04	0.02	0.4	3.96	—	—	—	—
α-SiC	0.03	—	—	—	—	—	0.2	3.2	0.58	0.05	0.22	3.5

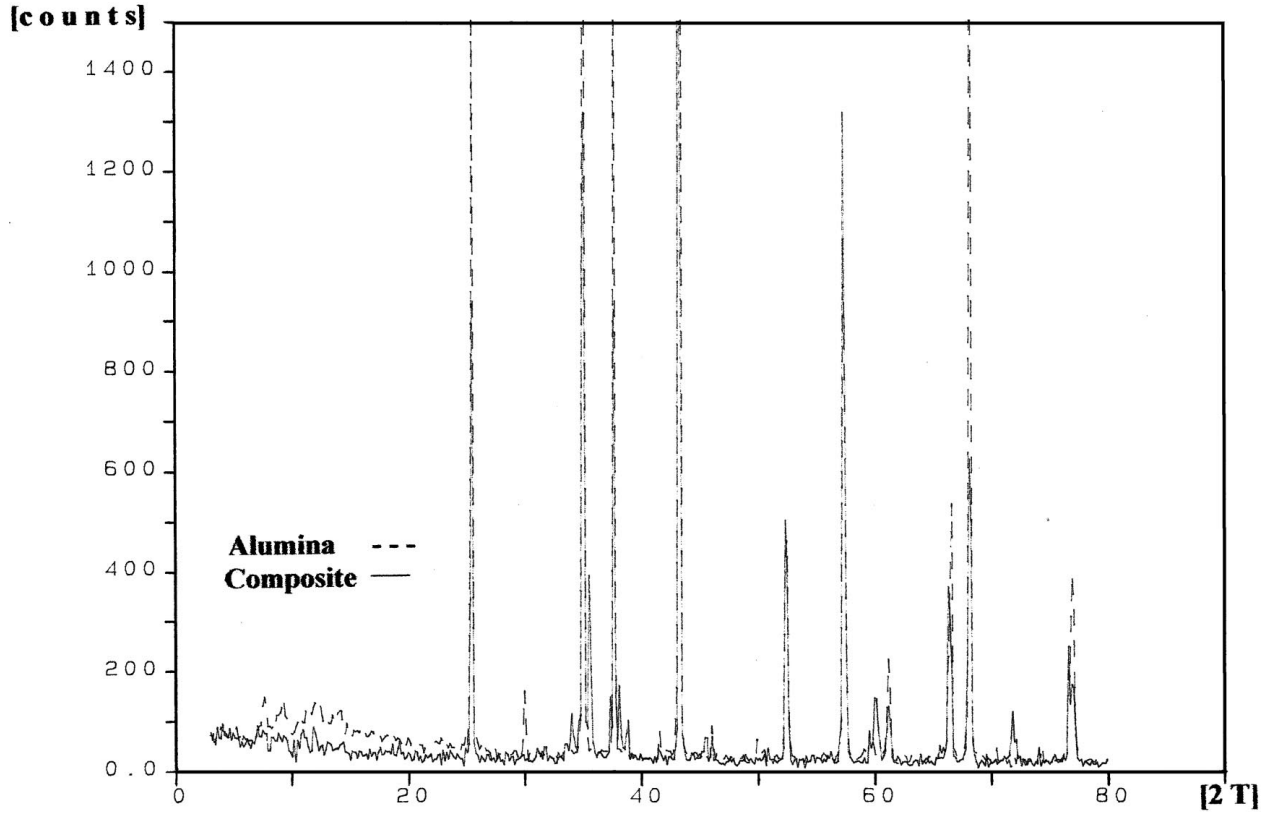

Figure 3 XRD of sintered monolithic Al_2O_3 (dashed line) and composites (full line) indicating—by the reduction of the hump between a 2θ value of about 7° and 15°—the reduction of silica rich phases in the bulk of composites.

out after each polishing stage from 14 μm down to 3 μm-finish (at which the chamfering was stopped). This method was adopted after observing that chamfering carried out after the faces have been polished ready for the test introduces scratches on the already polished faces. Five samples of each material were broken at room temperature. An Instron testing machine (model 1122), with a crosshead speed of 0.5 mm/min was used. The four-point bend jig had an inner span of 10 mm and an outer span of 20 mm. Fracture surfaces were studied using a Philips 501 SEM.

Every method used for the determination of K_{1C} presents its inaccuracies. For instance, in the SENB method a slight variation of the notch width introduces variations in the determined K_{1C} values [15]. However, the indentation method is quite popular due to its relative ease of application. Hence this method is used, of which the required conditions are that the crack length (*C*) must be ten times the average grain size of the sample and that the test surface is devoid of pre-existing stresses. To satisfy the latter samples were finish-polished to 1/4 μm (present work) and 3 μm diamond [2]. The K_{1C} of 1/4 μm finish-polished samples was found to be the same as that of 3 μm, hence an extract (for 5, 10 and 20 kg loads) of the values determined in reference [2] are used here, Table III. The table indicates that real differences exist between Al_2O_3 and the composites (as also have been observed by other authors [5, 6] on bulk samples) and between the composites. Although as with the Hertzian, Vickers indentation is also carried out on the surface, the difference is that cracks propagate in the latter. Hence Table III also indicates *R*-curve response in all the materials, which is fairly higher in the composites (5 and 10 vol % SiC grades)—a consequence of the effect of particles on crack propagation, which will be shown later.

TABLE III Vickers indentation K_{1C} ($MPa\,m^{1/2}$) of materials, function of loads

Load (kg)	Materials, vol % SiC			
	0, Al_2O_3	5	10	15
5	3.1 ± 0.3	4.3 ± 0.4	4.5 ± 0.3	4.8 ± 0.2
10	3.2 ± 0.2	4.6 ± 0.1	5.2 ± 0.2	5.5 ± 0.4
15	3.7 ± 0.2	5.3 ± 0.2	5.5 ± 0.3	5.7 ± 0.4

For the study of crack paths, and particularly their interaction to the scale of the sizes of the (nano) particles,

TEM is the only option. A technique similar to that used by Hockey [16], which does not seem to affect existing sub-structures was employed in the present work. Following this technique, Vickers indentations were made with 200-gram load on 200 μm-thick 3 mm-diameter discs of Alumina and the composites. None of the samples showed any residual stress cracking that sometimes occurs in ceramics after the load on the indenter is relaxed. The lengths of these cracks were not important for the TEM study, so no attempt was made to evaluate them, or any environmental effect on them between the indentation and milling processes.

The samples were then polished from the reverse of the indented side down to about 50 μm thickness discs. They were dimpled to about 20 μm thickness from the reverse sides before being ion-milled (using a Gatan Duomill) to produce a hole. The ion milling was first started with one gun (on the same reverse side) until a hole appeared. Both guns were then used (at a much lower angle) to remove the debris that had deposited on the other side of the disc when only one gun was in use.

Specimens were examined using a Philips CM 20 TEM. Imaging of dislocation structures was carried out under a two-beam condition for a rational comparison of them. Macro cracks in the TEM were imaged without tilting the samples.

3. Results and discussion

Table IV gives a summary of the four-point bend test results. The values of K_{1C} of the samples for 10 kg load [2], and associated critical flaw sizes are also included in this table. The fracture strength of all of the composites is higher than that of pure Alumina, decreasing with increasing volume fraction of SiC above 5%. The fracture toughness of all the composites is higher than that of pure Alumina, and slightly increases with increasing volume fraction of SiC above 5%. Mechanisms for the changes in strength and toughness are discussed below.

3.1. Reduction of SRP

Generally in pressureless sintering, relatively higher amounts of silica rich phases (SRP) permit the use of lower sintering temperatures to achieve a good densification, which otherwise is only possible at higher temperatures (as in the case of the composites here). On the other hand, higher amounts of SRP lead to reduced strength. Thus the bulk reduction of SRP in the composites (by the introduction of SiC particles) relative to monolithic Alumina of a similar grain size, Fig. 3, should contribute, albeit very small (given the initial content of about 0.1 wt % of SRP in the Alumina), to an increase in strength. The bulk reduction of SRP is more important in this regard, because it has been shown, for instance in Si_3N_4-SiC composite (with 8% Y_2O_3 sintering additive) [6], that the absence of SRP at particle-matrix interface alone does not lead to an increase in strength. The reduction of the bulk SRP makes it possible to obtain grains without abnormal growth.

TABLE IV Strength, K_{1C} values (10 kg load), density, grain sizes and critical flaw sizes of samples, C

Material, vol % SiC	Grain size [14] (μm)	Density, [14] % theoretical	σ_f (MPa)	K_{1C} [2] (MPa m$^{1/2}$)	C (μm)
0 (Al_2O_3)	3.5 ± 1.3	99.9	431 ± 53	3.2 ± 0.2	14 ± 7
5	4.0 ± 1.1	99.8	646 ± 41	4.6 ± 0.1	13 ± 7
10	2.9 ± 0.5	99.7	560 ± 8	5.2 ± 0.2	22 ± 4
15	2.6 ± 0.3	99.6	549 ± 30	5.5 ± 0.4	25 ± 8

3.2. Fracture modes

Fig. 4 shows SE micrographs, at a relatively low magnification, of the fracture surfaces of monolithic Alumina (4a), 5% (4b) and 15% (4c) SiC composites. While the fracture of monolithic Alumina is predominantly intergranular, that of the composites is mainly transgranular. Other authors [5, 6 and 12] have also observed this change in fracture mode. It is believed to be as a result of the high Al_2O_3/SiC interfacial energy in the composites, and it has been assumed that the change in fracture mode is connected with the increased strength and toughness of the composites [5]. The effect of high Al_2O_3/SiC interfacial energy is manifest at grain boundaries and inside the grains. At the former the cracks are forced to deflect into the grains. At the interfaces in the grains, the cracks undergo several processes (as will be shown in subsequent sections) that cumulatively lead to further cleavage facets.

Zhao *et al*. [12] argued that grain boundary modification from straight (Al_2O_3) to 'wavy' (composites) morphology prevents intergranular fracture. This geometric modification of boundaries was also observed [14] in the samples used in the present study. However, mode of fracture does not seem to have any relationship with grain boundary geometry. This is because it has been demonstrated in Alumina [17], and its composite with $LaAl_{11}O_{18}$ [18] that the same grain boundary geometry gives different modes of fracture, only as a function of grain size. Thus in comparison with small grain-sized ranges (<5 μm) large ones exhibit predominantly transgranular fracture. Therefore the predominance of transgranular failure in the composites of the present work, even at small grain sizes, should be due to Al_2O_3/SiC interface strength rather than grain boundary geometry.

Fig. 5 shows fracture surfaces of 5% and 15% SiC composites at higher magnification. Both fracture surfaces show steps on the transgranular cleavage facets (these are also visible in Figs 4b and 4c). The separation distance of the cleavage steps (some of which are labelled H_s) is 3.3 ± 1.1 μm in the 5% SiC composite (Fig. 5a), and 1.2 ± 0.4 μm in the 15% SiC composite (Fig. 5b).

3.3. Origins of cleavage steps from cracks

Cleavage steps could originate through the coalescence of smaller cracks, bifurcation of a fast running crack and/or local disturbances (possibly from the stiff SiC particles) experienced by primary cracks during their propagation [19]. In Figs 6a and b are transmission

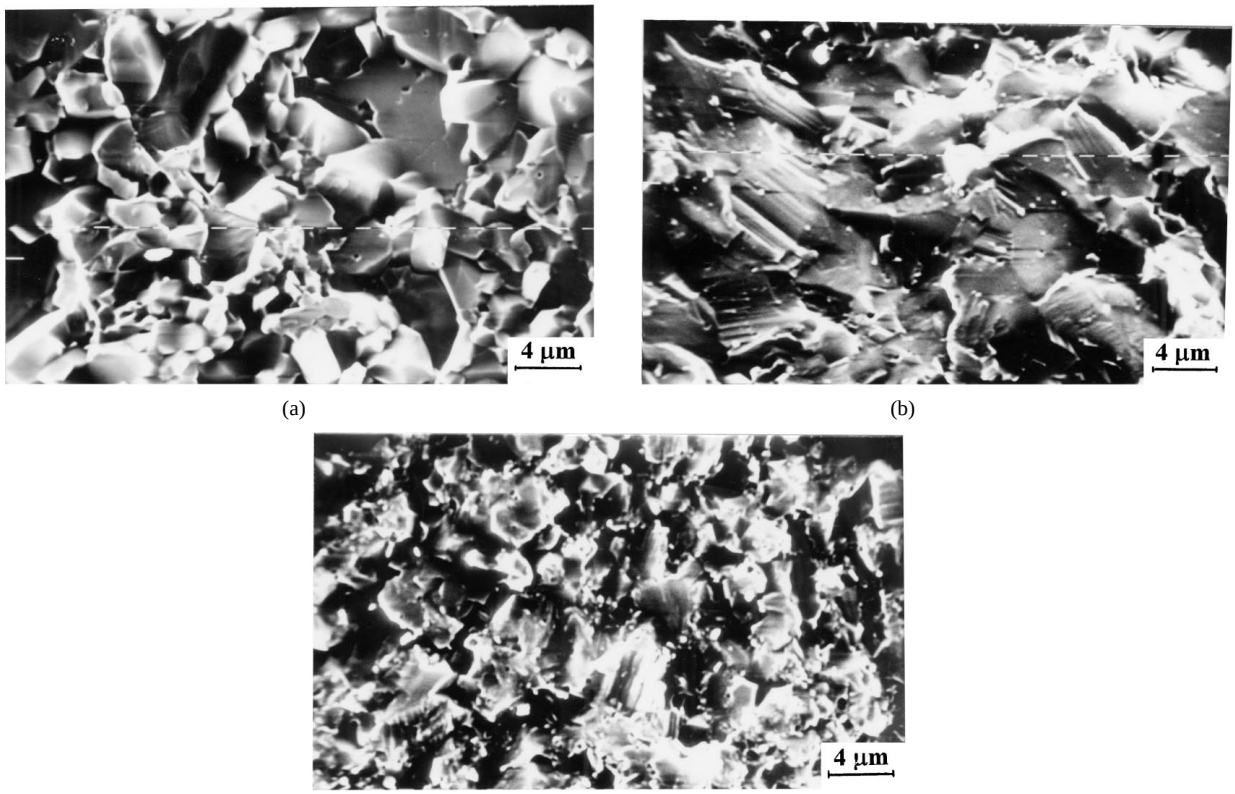

(a) (b)

(c)

Figure 4 Scanning Electron micrographs of fracture surfaces: (a) Alumina; (b) 5 vol %; and (c) 15 vol % composites. Alumina shows intergranular fracture. The composites show transgranular fracture. Note the higher density of cleavage steps in the 15 vol % SiC composite.

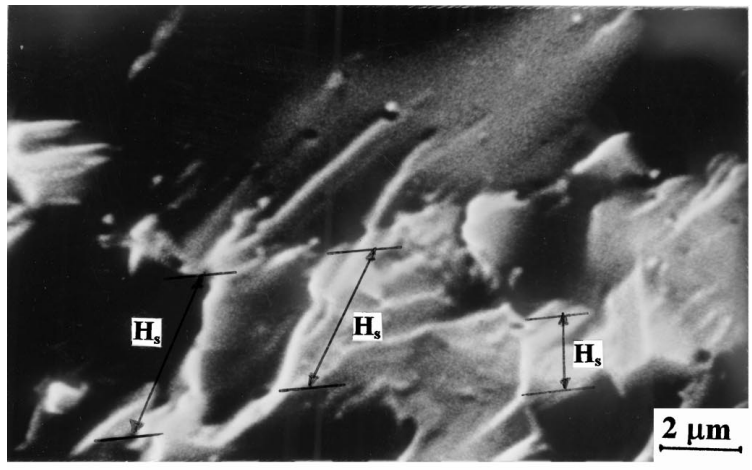

(a)

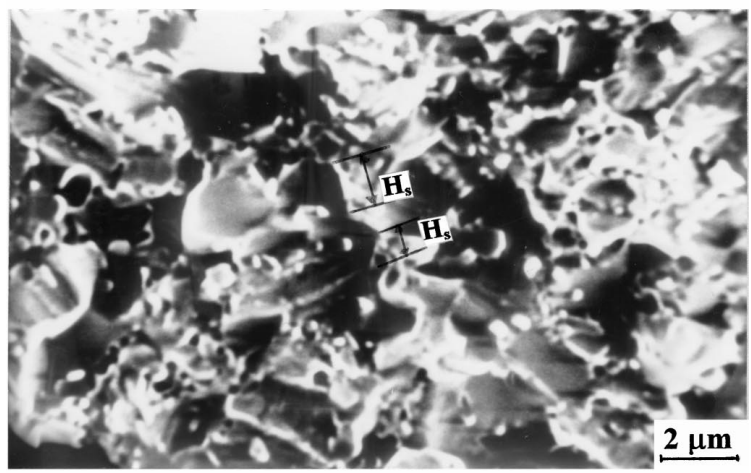

(b)

Figure 5 Higher magnification of Figs 4b and c, with samples tilted 3°. (a) 5 vol % SiC; (b) 15 vol % SiC composites. Note the bigger separation distances, H_s, of the cleavage steps in the 5% composite, relative to those in the 15% grade.

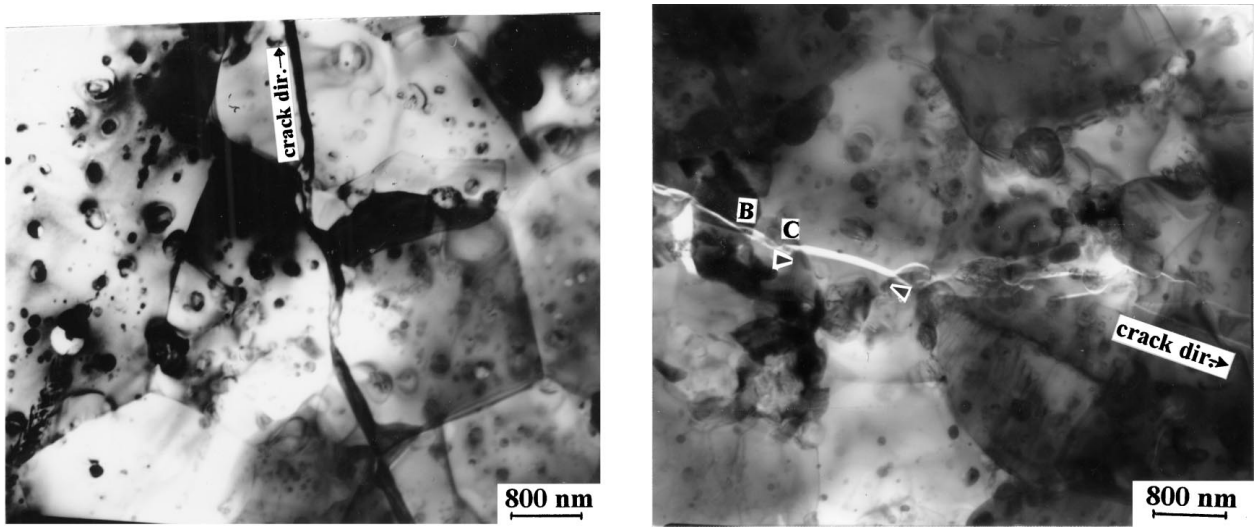

(a) (b)

Figure 6 TE micrographs of crack propagation in indented composite samples: (a) 5 vol % SiC; (b) 15 vol % SiC. Note the bifurcation (*B*) and coalescence (*C*) of cracks in the 15% grade; areas (an example is marked) not rich in particles have crack characteristics similar to those of 5 vol % grade.

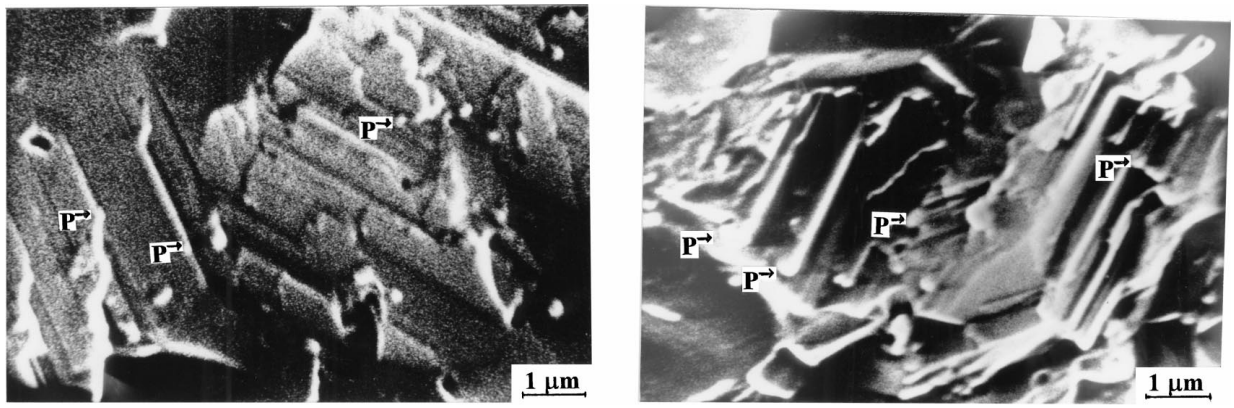

(a) (b)

Figure 7 SE micrographs of another view of the fracture surfaces showing the density of cleavage step: (a) 5 vol % SiC; (b) 15 vol % SiC composites. Note the higher particle (*P*) presence at edges of steps (see also Fig. 4b).

electron micrographs of the propagation of a crack in the 5% and 15% SiC composites, with the direction of the propagation, relative to the corner of the indent from which the crack emanates shown. (These directions are also shown in subsequent micrographs with crack propagation). The incidence of bifurcation (*B*) and coalescence (*C*) is higher in the 15% SiC composite than in the 5% composite, presumably due to a higher content of local obstacles (SiC particles). Even in the 15% SiC composite, areas locally less rich in particles (arrowed segment, Fig. 6b) tend to have less crack diversions. Hence these processes that as a result of strong Al_2O_3/SiC interface lead to the formation of steps inside the grains (precipitated by the particles in them) further enhance transgranular mode of crack propagation.

Fig. 7 shows fracture surface steps in the composites at higher magnification. The edges of some steps have some SiC particles (*P*), and the planar sections are virtually devoid of them (see also Fig. 4b), suggesting that the amount of stepping is controlled by the amount of particles present. The higher toughness of the composites relative to Alumina may be connected with the change from intergranular fracture (Alumina) to *stepped* transgranular cleavage (composites), Fig. 4. Each time a brittle crack front meets the steps, some of its energy is dissipated thus restraining its propagation. The density and height of the steps determine to what extent the cracks are restrained [19]. Thus the slight increase in toughness of the composites with higher volume fractions of SiC may be partly due to the higher density of these steps (compare Fig. 7a with Fig. 7b).

3.4. Particles as crack-stoppers and generators of dislocations

Fig. 8a shows an indentation crack being stopped at a particle (arrowed) in 5 vol % SiC composite. The crack appears to be attracted towards a particle and then to propagate round it. A similar effect in the 15% SiC material is shown in Fig. 8b. Note the bifurcation of the crack by the particle (*P*) before the arrest points (arrowed). Cracks are most likely to propagate along weak interfaces, for instance through the grain boundaries in monolithic Alumina, Fig. 8c. However, particle-Alumina interfaces have been shown

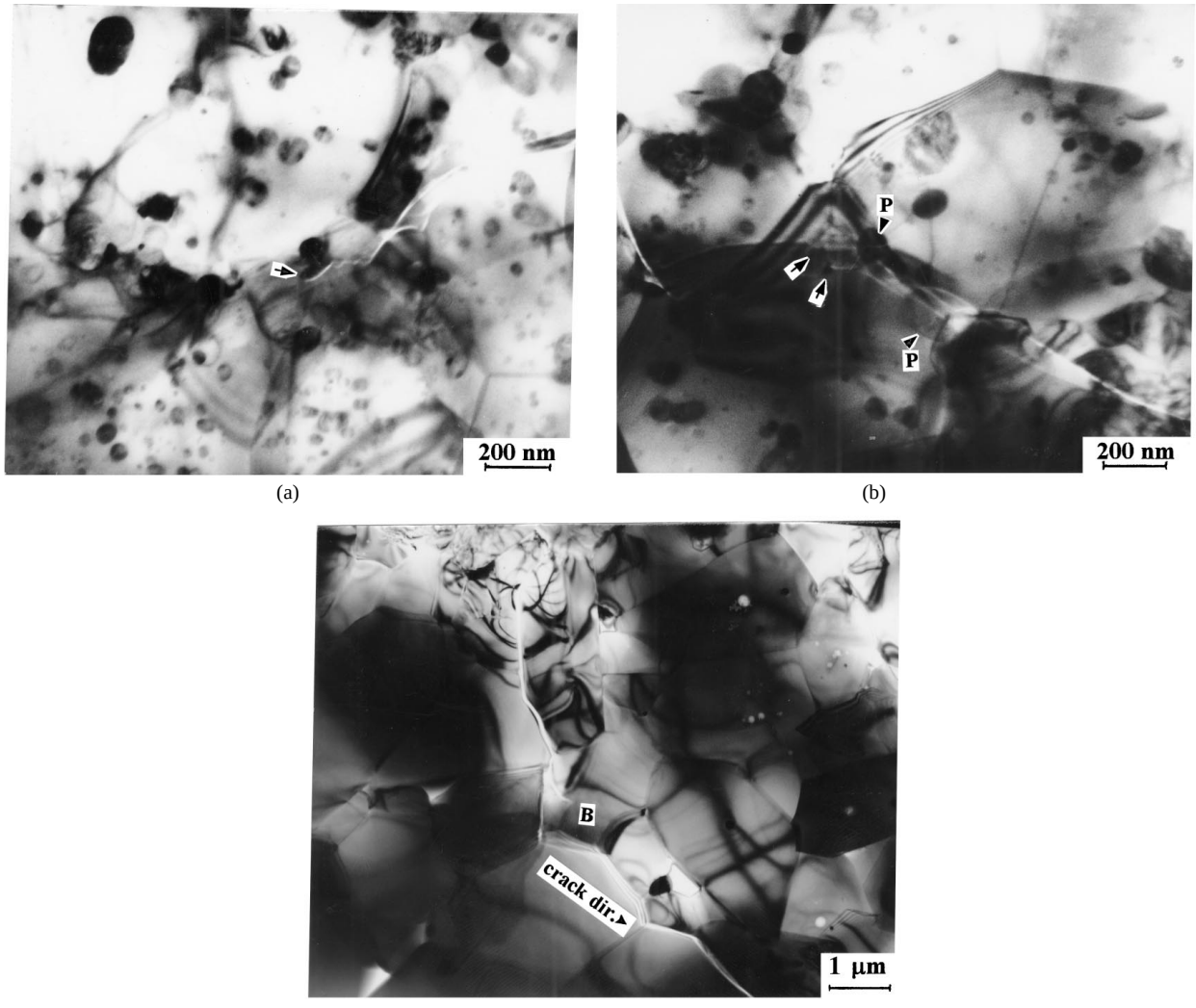

Figure 8 Attraction of cracks to: Particle-Alumina interfaces in (a) 5 vol %; (b) 15 vol % SiC composites; (c) grain boundaries in Alumina. Note that the tendency for cracks to bifurcate at Particles (*P*) in the 15 vol % SiC composite continues up to the arrest points (arrowheads). Note also that far fewer bridges (*B*) are found in Alumina relative to those found in the composites (Fig. 10).

[5] to be more strongly bonded than Alumina-Alumina interfaces. The attraction of the crack to the particle/Alumina interface may be as a result of local elastic stress fluctuations within the grain.

These stresses will be generated principally by the thermal expansion coefficient (α) mismatch between SiC particles and Alumina matrix during the cooling part of the sintering cycle. The stresses lead to radial microcracks [20], because $\alpha_p < \alpha_{matrix}$. However, the magnitude of the generated stress is such that it is not fully relieved through the microcracks, thus further relief is achieved through dislocation generation immediately around the particles, Fig. 9. The relief leads to local stress gradients between areas immediately around and farther away from the particles. This favours the propagation of a primary crack towards the weaker stress front immediately around the particle. But the crack is ultimately stopped by the stiff particle hence leading to a toughening effect.

Sometimes there is a tendency in Al_2O_3/SiC nanocomposites for the intergranular particles to be of larger sizes relative to the intragranular ones, irrespective of the particles' volume fractions, as was observed in this work (Fig. 6b) and that of Ohji *et al*. [5]. Some other times the intragranular particles are a mixture of both small and large particles, Fig. 9b. As the SiC content increases, it would be expected that the inter-particle distances would reduce. The effect of inter-particle distances (for a given volume fraction of particles) has been investigated by Carroll *et al*. [21], and they found no clear relationship of strength with this. As only one particle mean size was used in this work, the processing of the samples was not designed to obtain a particular mode of distribution of particle sizes. According to Zener's theory, grain boundary pinning obtains only when the particles are of some critical volume fraction and particle size. With regard to the latter, it should be expected that those particles less than, or very much above (usually isolated) this critical size would always be found within the grain since they can not effectively pin the boundaries. However, judging from Figs 6 and 9 the distribution is purely random, irrespective of particle content. But the micrographs reflect the particle size distribution of the powder, with d_{50} of about 200 nm. Therefore no attempt is made to relate the trends in K_{1C} and strength of the nanocomposite samples of the present work to inter and intragranular particle size distributions.

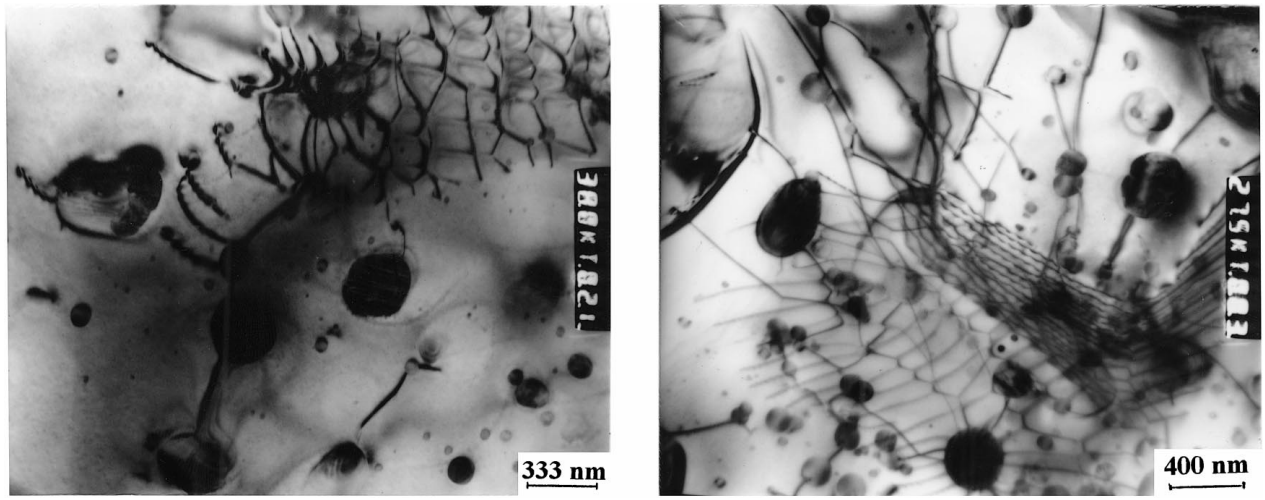

(a) (b)

Figure 9 Dislocations generated at the sintering stage in: (a) 5 vol %; (b) 15 vol % SiC composites. Some of these dislocations can be seen immediately around the particles interacting with cracks in Figs 8a and b.

3.5. Wake toughening

Any microstructural feature that restricts the relative movement of crack faces in the crack wake can lead to "wake toughening". In crack wake toughening, bridging features produce crack closure traction that reduces the stress at the crack tip, giving rise to the "*R*-curve" effect [22].

Fig. 10 shows examples of wake toughening in 5% SiC (Fig. 10a) and 15% SiC (Fig. 10b) composites. Bifurcation and coalescence of cracks, giving rise to ligaments that connect the crack surfaces, can arise inside the grains, particularly in the 15% SiC composite (grain *G* in Fig. 10b). When three particles touch, as is most probable in composites with higher volume fraction of particles, crack bridges can form, Fig. 10c (15% SiC composite). These phenomena dissipate the crack energy, thus restraining its propagation.

Wake toughening also obtains in monolithic Alumina, but the number of bridges appears to be fewer in Alumina (an example is marked B in Fig. 8c) than in the composites. In comparison with the grain-bridges found in Alumina, the fact that for a given volume of material, many more particle-bridges are found in the composites (compare Figs 10a and b with 8c) could be responsible for the stronger wake toughening effect of the particles. Again, the stiffer particle-bridge guarantees a far more extent of stable crack propagation than would the Alumina grain-bridge.

3.6. Critical flaw sizes

The effects of SiC particles on crack paths presumably lead to the observed increases in K_{1C} of the composites relative to pure Alumina. All the composites are stronger in bending than Alumina, though the strength decreases as SiC content rises, while the toughness increases slightly. It is necessary therefore to consider the connection between toughness and strength via the critical flaws present in the specimens. These flaws could arise during processing (sintering) or during surface preparation for mechanical tests.

The fracture stress, σ_f, of a brittle material with fracture toughness K_{1C} is given by:

$$\sigma_f = \frac{K_{1C}}{Y\sqrt{\pi C}} \tag{2}$$

where C is the critical (largest) flaw size present in the material, and Y is a geometrical constant, which is roughly equal to 1.12 [23, 24]. In Table IV are listed the critical flaw sizes from Equation 2, derived from the measured strength and K_{1C} values. The critical flaw sizes are similar for Alumina and the 5% composite, and then increase with SiC content.

The critical flaws are ten times larger than a typical grain, and their size is not directly related to grain size. Alumina and the 5% SiC composite have the largest grain sizes and the smallest critical flaws, while the 10% and 15% SiC composites have the smallest grain sizes and largest critical flaws. Fig. 11 shows an example of the tensile face finish ($1/4\ \mu$m diamond), in this case 15 vol % SiC composite, achieved in these samples. Such a finish suggests that the critical flaws are most unlikely to result from the surface, but rather from local defects introduced at the sintering stage. All the materials sintered to about the same high degree of densification ($99.7 \pm 0.2\%$ of their respective theoretical densities [14]). Alumina and 5 vol % SiC composite are virtually of the same critical flaw size, Table IV. Therefore explanations of high strength of the composites based on critical flaw sizes calculated on the basis of Griffith's relationship, for example, see references [6] and [21], are ambiguous. This is particularly so when all or any of the other mechanisms such as fracture mode, fractographic details and dislocation activities in a subsequent process (see the next section) across the samples under study differ(s).

Levin *et al*. [25] offered another possible explanation of the decrease of strength of a 15% SiC composite relative to a 5% SiC composite. They suggested that, due to the thermal expansion coefficient mismatch between Alumina and SiC, the matrix is in tension at large volume fractions of particles, and is thus liable to fracture

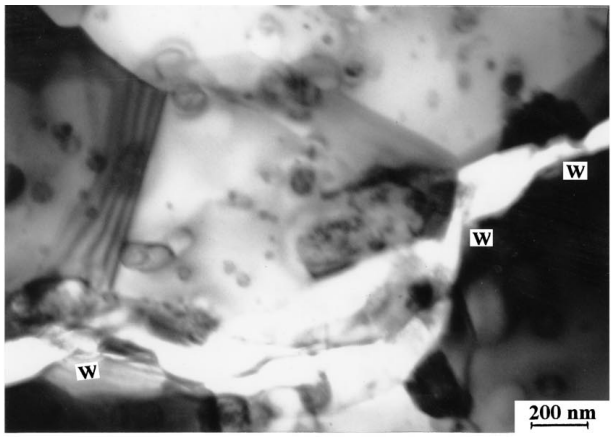

(a)

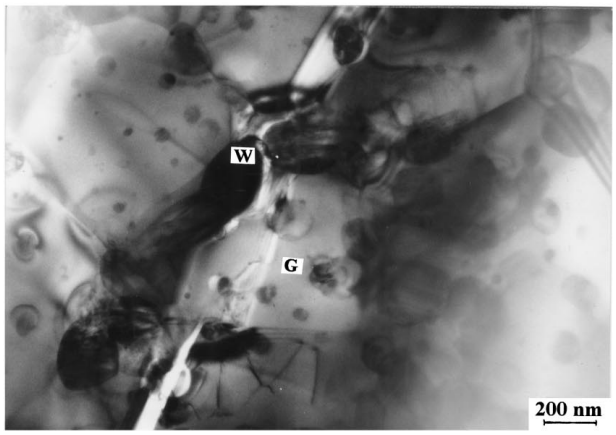

(b)

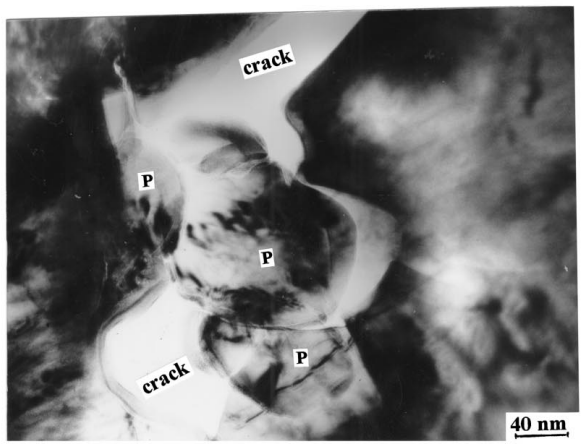

(c)

Figure 10 Crack deflection, bifurcation and wake toughening (*W*) in: (a) 5 vol %; (b) 15 vol % SiC composites. '*G*' indicates where bridging occurs inside a grain. (c) Crack bridging by three particles in 15% composite.

at lower stresses. The effect of small flaws on K_{1C} is not certain. However, it is known [22] that microcracks (arising from the tension in the matrix)—particularly at the nanoscale they are found [20] in composites of the present work—lower the strain energy of primary crack tips having their stress fields within them, thus increasing the toughness slightly. Borsa *et al*. [26] found an increase in strength beyond 5% SiC addition, which they suggested was due to grain growth inhibition by high SiC fractions. Although higher amounts of SiC addition did give finer grain, this did not lead to higher strength in the materials of the present work.

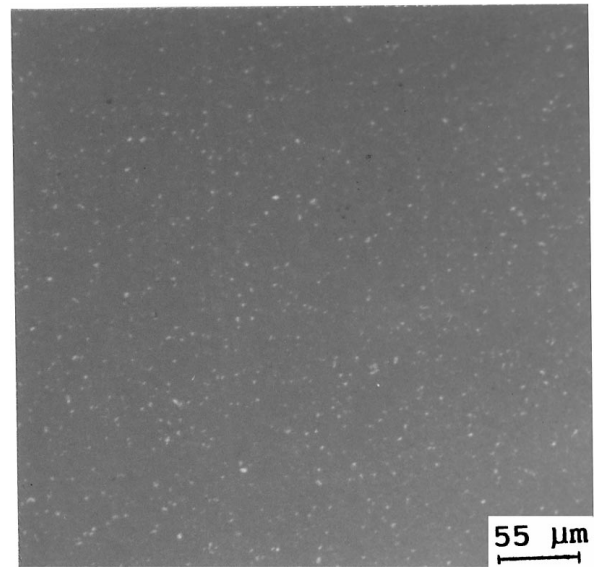

Figure 11 Optical micrograph of a tensile face of 15 vol % SiC composite finish-polished to $1/4\,\mu$m diamond typifying the surface finish achieved in all the samples.

4. Strength and toughness of annealed composites (dislocation mechanism)

As was demonstrated in Section 1, the explanation of strength increase (observed by other authors in annealed composites [1, 6 and 12]) based on healable flaws is inconsistent. It has been suggested [6] that the remarkable improvement of the fracture strength by annealing is due to further development of sub-grain boundaries during the process. Therefore a better explanation could be found in the activity of the dislocations that were generated in the composites at the sintering, Fig 9, and the grinding stages during the annealing process.

"Surface" dislocations are generated in grinding/machining processes (with compressive stresses) of Alumina and the nanocomposite, to a minimum depth of the samples, as has been demonstrated by several authors [3, 16, 27]. These "surface" dislocations (using Vickers load as low as 2N) were found [3] within a maximum area of about 10 μm radius of the indent for the composite, and slightly shorter for Alumina. Their network structure differed substantially from that of bulk dislocations (obtained at the sintering stage).

In Table I it can be seen that the polished sample (with virtually no "surface" dislocations) showed a lower strength than the ground sample annealed for the same period of ten hours. Apart from the additional "surface" network from the machining process of the ground sample, the (bulk) dislocation structure of these two samples from the sintering stage is the same. It can be seen that in the absence of a difference in other mechanisms that affect strength, in unannealed condition flaw size is the controlling factor. Thus the polished sample, with smaller critical flaw sizes, is stronger. However, after annealing, because of the development of sub-grain boundaries by dislocations, flaw size factor becomes unimportant; the ground sample now levels up, and then even becomes stronger than the polished sample. It is now stronger due to its additional "surface" dislocation

network. The small difference in strength of $11 \pm 4\%$, induced by the "surface" dislocation network indicates that indeed the bulk dislocation structure is controlling. Further support to this hypothesis can be found in the work of Fang *et al*. [28] on annealed Alumina and nanocomposite. Whereas the former has dislocation-free sub-grains, dislocation entanglement remains in the nanocomposite.

Annealing reduces local stress gradients. Thus the observed preferential attraction of a propagating primary crack to areas immediate to the particles (Fig. 8a), which had its local stress relatively low in deformed unannealed sample is reduced. So also is the role of the particles as crack-stoppers. It is also very likely that annealing heals the sub-micron-sized radial flaws (typically about 150 nm [20]) that were created at the sintering stage. Hence their effect in blunting the tip of a propagating crack is minimised. The cumulative effect of these on the K_{1C} of annealed composites is that of a slight reduction in its value. Thus Zhao *et al*. [12] observed a slight reduction in toughness of about 8% (with an increase in strength of about 32%).

5. Study of strengthening in nanocomposites using Scanning Acoustic Microscope, SAM (Scanning Acoustic Waves, SAW).

From the foregoing it is evident that the impact of flaws on strength (when applicable) is primarily through the critical sizes and to a lesser degree, the density of the flaws. At 2 GHz a typical resolution limit of a SAM is 700 nm [29], so at 225 MHz [1] the resolution limit is bound to be poorer than 700 nm. Thus it is incapable of detecting the sub-micron-sized flaws (of about 150 nm) and particles present in these samples. Therefore their effect is not reflected in the SAW velocities that are used to draw conclusions on the role of interfaces or cracks in these materials.

An important precondition [30] for using SAM to characterise materials is that the sample should be well polished. Wu *et al*. [1] used the technique on ground samples, which is not in conformance with the precondition. Thus the conclusions from such a non-conformant procedure are unreliable.

The SAM method has also been demonstrated [31] to be insensitive to critical flaw sizes. It therefore cannot throw any light on the primary route through which flaws have impact on strength. Furthermore, it is evident from this work that in the presence of other mechanisms the role of flaws as a strength-controlling factor is relegated. The SAM method is incapable of studying these other mechanisms such as fractographic details and dislocation networks. For these reasons the method is unsuitable for these materials.

6. Conclusions

Microstructural features have been used to explain the strengthening and toughening of Al_2O_3-$SiC_{(p)}$ composites of varying volume fraction of SiC nano-particles, and relative to monolithic Alumina.

Four-point bend flexural strength of the composites (550–650 MPa) is higher than that of monolithic Alumina (∼430 MPa), and decreases slightly as the volume fraction of SiC particles is increased beyond 5%. The critical flaw sizes in the materials, derived from measured fracture stresses and K_{1C} values, were found to increase slightly with the volume fraction of particles above 5% SiC. The critical flaw sizes (∼15–25 μm) were much larger than a typical grain diameter (2.5–3.5 μm), and the flaw size bore no relationship with grain size. No critical flaw size of the order predicted by standard fracture mechanics was observed on the polished faces. In the presence of other mechanisms (for example, fracture mode), flaw size is relegated as a strength-controlling factor. The addition of SiC particles (with the associated free carbon) reduces the amount of silica rich phases, which in turn could contribute to higher strength in the composites.

In unannealed condition the K_{1C} values of the composites (5–5.5 MPa $m^{1/2}$) are higher than that of monolithic Alumina (∼3.5 MPa $m^{1/2}$), and they increase slightly as the volume fraction of SiC particles increases (up to 15% SiC in this study). The increase in the K_{1C} values may be connected with steps on transgranular fracture surfaces; these steps appear to result from crack-particle interactions and increase in density with increasing SiC content. Cracks may also be trapped at particles and their tips may be blunted by clusters of sub-micron-sized flaws, further contributing to an increase in K_{1C}.

From experimental observations the idea of increased dislocation activities being responsible for the increase in strength in annealed composites appears to be more consistent than that of flaw healing. More experiments with annealed near fully dense composites with >5% SiC nano-particles (higher dislocation density) may be necessary for further confirmation.

Owing to the nanometric scale of the features that control strength in these composites and the very nature of Scanning Acoustic Microscopy (Waves) the latter may not be a good method for studying strength trends in these materials.

Acknowledgement

This work was supported by the EPSRC, UK.

References

1. H. Z. WU, C. W. LAWRENCE, S. G. ROBERTS and B. DERBY, *Acta Mater*. **46** (1998) 3839.
2. C. C. ANYA and S. G. ROBERTS, *J. Euro. Ceram. Soc.* **16**(10) (1996) 1107.
3. C. C. ANYA, *J. Mater. Sci.* **33** (1998) 977.
4. I. A. CHOU, H. M. CHAN and M. P. HARMER, *J. Amer. Ceram. Soc.* **79** (1996) 2403.
5. T. OHJI, T. HIRANO, A. NAKAHIRA and K. NIIHARA, *ibid*. **79**(1) (1996) 33.
6. K. NIIHARA, *J. Ceram. Soc. Jpn.* **99**(10) (1991) 974.
7. T. NOSE and T. FUJII, *J. Amer. Ceram. Soc.* **71**(5) (1988) 328.
8. K. NIIHARA, A. NAKAHIRA, G. SASAKI and M. HIRABAYASHI, in "Proceed. Mater. Res. Soc. on Advanced Mater.," Vol. 4, edited by M. Doyama, S. Somiya and R. P. H. Chang (Mater. Res. Soc. Pittsburgh, PA, 1989) p. 129.
9. K. NIIHARA and A. NAKAHIRA in "Proceed. 3rd Intl. Symp. on Ceramic Materials and Components for Engines," edited by V. J. Tennery, (Amer. Ceram. Soc. Westerville, OH, 1988) 919.

10. K. NIIHARA and A. NAKAHIRA, in "Advanced Structural Inorganic Composites," edited by P. Vincentini (Elsevier, Trieste, Italy, 1990) p. 637.
11. J. OTSUKA, S. IIO, Y. TAJIMA, M. WATANABE and K. TANAKA, *J. Ceram. Soc. Jpn.* **102** (1994) 29.
12. J. ZHAO, L. C. STEARNS, M. P. HARMER, H. M. CHAN and G. A. MILLER, *J. Amer. Ceram. Soc.* **76**(2) (1993) 503.
13. Y. IKUMA and A. V. VIRKAR, *J. Mater. Sci.* **19** (1984) 2233.
14. C. C. ANYA and S. G. ROBERTS, *J. Euro. Ceram. Soc* **17**(4) (1997) 565.
15. J. C. GLANDUS, T. ROUXEL and Q. TAI, *Ceram. Intnal.* **17** (1991) 129.
16. B. J. HOCKEY, *J. Amer. Ceram. Soc.* **54** (1971) 223.
17. B. MUSSLER, M. V. SWAIN and M. CLAUSEN, *ibid.* **65**(11) (1982) 566.
18. H. L. O'DONNELL, M. J. READEY and D. KOVAR, *ibid.* **78**(4) (1995) 849.
19. B. LAWN, "Fracture of Brittle materials," 2nd Ed. (Cambridge Univ. Press, Cambridge, UK, 1993) p. 194.
20. C. C. ANYA, *J. Mater. Sci. Lttrs.* **16** (1997) 1300.
21. L. CARROLL, M. STERNITZKE and B. DERBY, *Acta Mater.* **44**(11) (1996) 4543.
22. F. L. MATTHEWS and R. D. RAWLINGS, "Composite Materials: Engineering and Science," (Chapman and Hall, London, 1994) chap. 11.
23. M. SAKAI and R. C. BRADT, *Intl. Mats. Review* **38**(2) (1993) 53.
24. R. W. DAVIDGE, "Mechanical Behaviour of Ceramics," (Cambridge Univ. Press, Cambridge UK, 1986) 31.
25. I. LEVIN, W. D. KAPLAN, D. G. BRANDON and T. WEIDER, *Acta Metall. Mater.* **42**(4) (1994) 1147.
26. C. E. BORSA, S. JIAO, R. I. TODD and R. J. BROOK, *J. Micros.* **177**(3), (1995) 305.
27. B. R. LAWN, B. J. HOCKEY and S. M. WIEDERHORN, *J. Mater. Sci.* **15** (1980) 1207.
28. J. FANG, H. M. CHAN and M. P. HARMER, *Mater. Sci. Eng., A* **195** (1995) 163.
29. C. W. LAWRENCE, G. A. D. BRIGGS and C. B. SCRUBY, *J. Mater. Sci.* **28** (1993) 3645.
30. *Ibid.*, 3635.
31. P. D. WARREN, C. W. LAWRENCE, S. G. ROBERTS, G. A. D. BRIGGS, C. PECORARI, O. V. KOLOSOV and M. M. PUENTES-HERAS, *British Ceram. Procd.* **57** (1996) 167.

Received 18 June 1998
and accepted 27 April 1999